

Hemodynamic Deconvolution Demystified: from Paradigm Free Mapping to Total Activation

Eneko Uruñuela^{a,b,*}, Thomas A.W. Bolton^{c,d}, Younes Farouj^d, Dimitri Van de Ville^{d,e}, César Caballero-Gaudes^a

^a*Basque Center on Cognition, Brain and Language (BCBL), Donostia-San Sebastián, Spain.*

^b*University of the Basque Country (EHU/UPV), Donostia-San Sebastián, Spain.*

^c*Gamma Knife Center, Department of Clinical Neuroscience, Centre Hospitalier Universitaire Vaudois (CHUV), Lausanne, Switzerland*

^d*Swiss Federal Institute of Technology Lausanne (EPFL), Lausanne, Switzerland.*

^e*Faculty of Medicine of the University of Geneva, Geneva, Switzerland*

Abstract

Deconvolution of the hemodynamic response is an important step to access short timescales of brain activity recorded by fMRI. Albeit conventional deconvolution algorithms are around since a long time (e.g., Wiener deconvolution), recent state-of-the-art methods based on sparsity-pursuing regularization are attracting increasing interest to investigate brain dynamics. This technical note revisits the main concepts underlying two main methods, paradigm free mapping and total activation, in the most accessible way. Despite their apparent differences, these methods are theoretically equivalent as they represent the synthesis and analysis sides of the same problem. We demonstrate this equivalence in practice with their best-available implementations using both simulations, with different signal-to-noise ratios, and experimental data of motor task and resting-state fMRI. We evaluate the parameter settings that lead to equivalent results, and benchmark the computational speed of both algorithms. This note is useful for practitioners interested to better understand state-of-the-art hemodynamic deconvolution, and want to make use of the most efficient implementation.

Keywords: fMRI deconvolution, paradigm free mapping, total activation

1. Introduction

Functional magnetic resonance imaging (fMRI) data analysis is often directed to disentangling and understanding the neural processes that occur among brain regions. While interactions in the brain are electrical in nature, the blood oxygenation level-dependent (BOLD) signal present in fMRI data reflects hemodynamics. Thus, an intermediate step that estimates the underlying neuronal activity from the BOLD signal can prove to be useful for understanding such interactions. Often, the analysis of task fMRI data relies on generalized linear models (GLM) to detect maps of brain activity by using the information about the timings of the BOLD events. However, this information can be unknown, inaccurate, or insufficient in some scenarios. In such cases, and given the nature of the BOLD signal, the appropriate approximation of the neuronal activity can be obtained by means of deconvolution with an assumed hemodynamic response (Gitelman et al. 2003).

Deconvolution and methods alike are becoming more popular for exploring time-varying activity in fMRI data within a number of neuroimaging studies due to their potential to blindly disentangle neural dynamics. One of such

cases is the study of resting-state fluctuations with the aim of gaining insight into the origin of the signals driving functional connectivity and its temporal dynamics, as well as the organizational principles of brain function; i.e., to study and deconstruct the spatio-temporal structure of functional components that dynamically construct resting-state networks (Petridou et al. 2013; Karahanoğlu and Van De Ville 2015, 2017; Kinany et al. 2020; Gonzalez-Castillo et al. 2019; Allan et al. 2015; Esfahlani et al. 2020). Another case in which the timing of the BOLD events is unknown is that of naturalistic paradigms, where subjects are shown a movie or story with the aim of detecting the functional structure of shared responses among a group of subjects and idiosyncratic patterns that could reveal meaningful individual differences (Finn and Bandettini 2020; Finn et al. 2020; Betzel et al. 2020; Faskowitz et al. 2020). Furthermore, deconvolution techniques can probe to be helpful in clinical conditions to characterize functional alterations of patients with a progressive stage of multiple sclerosis at rest (Bommarito et al. 2020), to find functional signatures of prodromal psychotic symptoms and anxiety at rest on patients suffering from schizophrenia (Zöller et al. 2019), to detect the foci of interictal events in epilepsy patients without an EEG recording (Lopes et al. 2012), or to study functional dissociations observed during non-rapid eye movement sleep that are associated with reduced consolidation of information and impaired consciousness

*Corresponding author

Email address: e.urunuela@bcbl.eu (Eneko Uruñuela)

(Tarun et al. 2020).

This note describes and compares synthesis- and analysis-based deconvolution methods for fMRI data and comprises three sections. In the first, we present the theory behind two state-of-the-art deconvolution approaches based on L1-norm regularized estimators: Paradigm Free Mapping (PFM) (Caballero Gaudes et al. 2013) — available as *3dPFM* and *3dMEPFM* in AFNI — and Total Activation (TA) (Karahanoglu et al. 2013) — available as part of the *iCAPs toolbox*. We then assess their performance using the same hemodynamic response function with different criteria for the selection of the regularization parameter. We report that both methods produce identical results when estimating the underlying activity-inducing and innovation signals in different signal-to-noise ratio (SNR) settings, and task-based and resting-state experimental datasets. In the final section, we discuss the pros and cons of each of the described techniques and conclude with our vision on potential extensions and developments for deconvolution algorithms for fMRI.

2. Theory

The hemodynamic response to neuronal activity at time t can be modeled as the convolution with a finite impulse response function of the neuronal signal $s_{t-\tau}$ at time $t-\tau$ with the hemodynamic response function h_τ (Gitelman et al. 2003):

$$y_t = \sum_t h_\tau s_{t-\tau}, \quad (1)$$

where y_t is the measured BOLD signal on a given voxel v . This equation can be reformulated in matrix notation as $\mathbf{y} = \mathbf{H}\mathbf{s} + \epsilon$, where $\mathbf{y}, \mathbf{s} \in \mathbb{R}^N$, $\mathbf{H} \in \mathbb{R}^{N \times N}$ is the HRF in Toeplitz matrix form, N is the number of frames of the fMRI acquisition, and ϵ represents additional white Gaussian noise. The signal model in (1) can be extended to represent the neuronal signal \mathbf{s} in terms of its innovation signal \mathbf{u} , i.e., its derivative, as $\mathbf{s} = \mathbf{L}\mathbf{u}$ where $\mathbf{L} \in \mathbb{R}^{N \times N}$ is an integration operator (Cherkaoui et al. 2019; Uruñuela et al. 2020).

Functional MRI data analyses are often directed to disentangling and understanding the neural processes that occur among brain regions. However, interactions in the brain are expressed, not at the level of hemodynamic responses, but at the neural level. Thus, an intermediate step that estimates the underlying neuronal activity is necessary for such analyses. Given the nature of the fMRI BOLD signal, the appropriate approximation of the neuronal activity can be obtained by means of deconvolution with an assumed hemodynamic response (Gitelman et al. 2003). Hence, the maximum likelihood estimate of the hemodynamic response to the underlying neural activity can be calculated using the ordinary least-squares estimator that minimizes the residual sum of squares between the modeled ($\mathbf{H}\mathbf{s}$) and measured (\mathbf{y}) signals. Yet, the estimates of the neuronal activity \mathbf{s} must be constrained with

a regularization term to attenuate the collinearity and high variability of the design matrix \mathbf{H} .

2.1. Synthesis-based deconvolution

Paradigm Free Mapping (PFM) builds upon the signal model introduced in (1); i.e., the BOLD signal is the result of convolving the underlying neural activity with the hemodynamic response, and proposes to estimate the activity-inducing signal by solving the following regularized least-squares problem (Caballero Gaudes et al. 2013; Uruñuela et al. 2020; Gaudes et al. 2011):

$$\hat{\mathbf{s}} = \arg \min_{\mathbf{s}} \frac{1}{2} \|\mathbf{y} - \mathbf{H}\mathbf{s}\|_2^2 + \Omega(\mathbf{s}), \quad (2)$$

where $\Omega(\mathbf{s})$ is the regularization term.

Assuming that single-trial BOLD responses are the result of brief bursts of neuronal activation, the activity-inducing signal \mathbf{s} must be a sparse vector. Thus, sparse estimates of \mathbf{s} could be obtained by substituting $\Omega(\mathbf{s})$ in (3) with an l_0 -norm and solving the optimization problem (Bruckstein et al. 2009). However, due to the convolution model defined in (3), finding the optimal solution to the problem demands an exhaustive search across all possible combinations of the columns of the design matrix \mathbf{H} . Hence, a pragmatic solution is to solve the optimization problem with the use of an l_1 -norm, or LASSO (Tibshirani 1996), which is a convex function and therefore provides fast convergence to the optimal solution.

$$\hat{\mathbf{s}} = \arg \min_{\mathbf{s}} \frac{1}{2} \|\mathbf{y} - \mathbf{H}\mathbf{s}\|_2^2 + \lambda \|\mathbf{s}\|_1, \quad (3)$$

where λ regulates how sparse the optimal solution is.

Such formulation provides flexibility to expand the capabilities of PFM. For instance, incorporating the integration operator \mathbf{L} into the design matrix \mathbf{H} allows the recovery of the innovation signal \mathbf{u} ; i.e., the derivative of the activity-inducing signal \mathbf{s} . Therefore, the innovation signal can be estimated by solving the following optimization problem (Cherkaoui et al. 2019; Uruñuela et al. 2020):

$$\hat{\mathbf{u}} = \arg \min_{\mathbf{u}} \frac{1}{2} \|\mathbf{y} - \mathbf{H}\mathbf{L}\mathbf{u}\|_2^2 + \lambda \|\mathbf{u}\|_1. \quad (4)$$

2.2. Analysis-based deconvolution

Even though based on the same signal model as PFM, Total Activation (TA) proposes to use a linear differential operator L_h that inverts the hemodynamic system based on activelets to recover the activity-inducing signal \mathbf{s} (Karahanoglu et al. 2013; Khalidov et al. 2011; Karahanoglu et al. 2011):

$$L_h\{x\}(t) = s(t) \quad (5)$$

where x is the neuronal-related signal; i.e., the activity inducing signal \mathbf{s} convolved with the HRF, and L_h is defined as

$$L_h = \prod_{i=1}^{M_1} (D - \alpha_i I) \left(\prod_{j=1}^{M_2} (D - \gamma_j I) \right)^{-1}, \quad (6)$$

where D is the derivative operator, $\alpha_i (i = 1, \dots, M_1)$ define the zeros of the filter, $\gamma_j (j = 1, \dots, M_2)$ represent the poles, I is the identity matrix and $M_1 > M_2$. Given the relationship between the activity-inducing and the innovation signal, the latter can be recovered as:

$$L\{x\}(t) = D\{s\}(t) = u(t) \quad (7)$$

where $L = DL_h$ and D is the derivative.

Therefore, for a given voxel, the neuronal-related signal could be estimated by solving the following regularized least-squares problem:

$$\hat{\mathbf{x}} = \arg \min_{\mathbf{x}} \frac{1}{2} \|\mathbf{y} - \mathbf{x}\|_2^2 + \Omega(\mathbf{x}), \quad (8)$$

where \mathbf{y} is the fMRI data and $\Omega(\mathbf{x})$ is the following l_1 -norm regularization term:

$$\hat{\mathbf{x}} = \arg \min_{\mathbf{x}} \frac{1}{2} \|\mathbf{y} - \mathbf{x}\|_2^2 + \lambda \|\Delta_L \{\mathbf{x}\}\|_1, \quad (9)$$

where λ is the regularization parameter.

This work evaluates the core of the two techniques, i.e., the regularized least-squares problem with temporal regularization, which corresponds to the generalized total-variation operator in Total Activation. Thus, we do not study the impact of spatial constraints, as we assume that spatial regularization terms should perform identically on both methods.

140

3. Results

A critical decision with deconvolution methods is the selection of the regularization parameter λ , for which many techniques have been proposed in the literature but an optimal is yet to be discovered. In fact, Paradigm Free Mapping and Total Activation base their selection of the regularization parameter on different criteria: the Bayesian Information Criterion (BIC) (Schwarz 1978) and Akaike Information Criterion (AIC) (Akaike 1998), and a selection based on the convergence of the residuals to a pre-estimated level of the noise, respectively. Hence, we compare the performance of the two algorithms with both selection criteria. Furthermore, we explore the differences between the techniques in terms of the estimation of the activity-inducing signal \mathbf{s} using the *spike model* in (3) and the innovation signal \mathbf{u} using the *block model* in (4).

3.1. Simulated and experimental data

In order to compare the two methods while controlling for their correct performance, we simulated a 400 seconds ($TR = 2$ s) activity-inducing signal with five neuronal events, convolved it with the canonical HRF, and we added noise of different sources (physiological, thermal, and motion-related) with different signal-to-noise ratios ($SNR = [20 \text{ dB}, 10 \text{ dB}, 3 \text{ dB}]$) that represent low, medium and high levels of noise as shown in Figure 1.

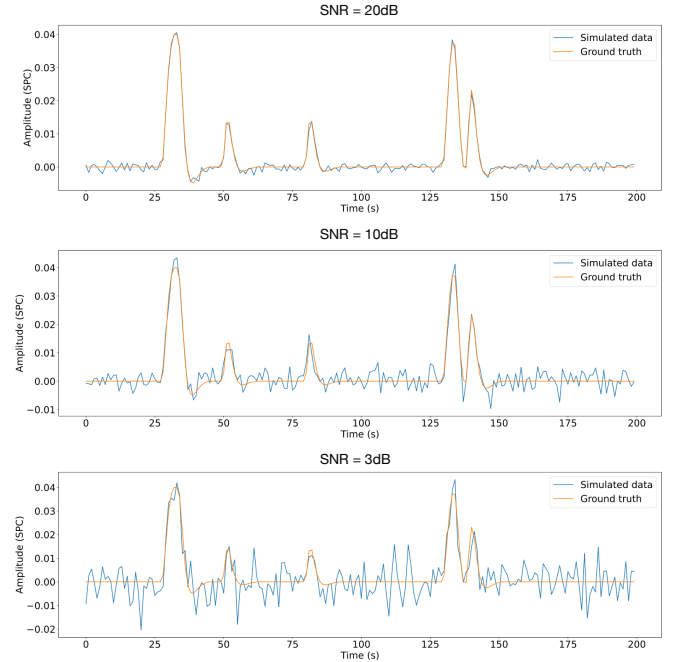


Figure 1: Simulated signal with different SNRs (20 dB, 10 dB and 3 dB).

Furthermore, we compared the two techniques on three datasets: a motor task and two resting-state acquisitions.

Motor task dataset: One healthy subject was scanned in a 3T MR scanner (Siemens) as part of a larger experiment under a Basque Center on Cognition, Brain and Language Review Board-approved protocol. T2*-weighted multi-echo fMRI data was acquired with a multiband (MB) multi-echo gradient echo-planar imaging sequence (340 scans, 52 slices, Partial-Fourier = 6/8, voxel size = 2.4x2.4x3 mm³, TR = 1.5 s, TEs = 10.6/28.69/46.78/64.87/82.96 ms, multiband factor = 4, flip angle = 70°, GRAPPA = 2). During the fMRI acquisition, subjects performed a motor task consisting of five different movements (left-hand finger tapping, right-hand finger tapping, moving the left toes, moving the right toes and moving the tongue). These conditions were randomly intermixed every 16 seconds, and were only repeated once the entire set of stimuli were presented. Data preprocessing consisted of optimally combining the echo time datasets, detrending of up to 5th-order Legendre polynomials, spatial smoothing (3 mm FWHM) and normalization to signal percentage change. For this comparison, we selected a voxel that best represented the right-hand finger-tapping paradigm based on a generalized linear model as shown in Figure 2.

Resting-state datasets: One healthy subject was scanned in a 3T MR scanner (Siemens) as part of a larger experiment under a Basque Center on Cognition, Brain and Language Review Board-approved protocol. Two runs of T2*-weighted fMRI data were acquired during resting-state, each with 10 min duration, with 1) a standard gradient-

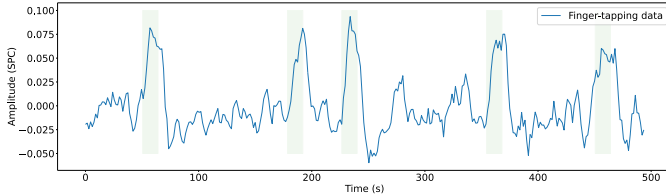


Figure 2: Most representative voxel of the finger-tapping task. Green blocks indicate the onsets and the duration of it.

echo echo-planar imaging sequence (monoband) ($TR = 2000$ ms, $TE = 29$ ms, flip-angle = 78° , matrix size = 64x64, voxel size = $3 \times 3 \times 3$ mm 3 , 33 axial slices with interleaved acquisition, slice gap = 0.6 mm) and 2) a simultaneous multislice gradient-echo echo-planar imaging sequence (multiband factor = 3) developed by the Center of Magnetic Resonance Research (University of Minnesota, USA; $TR = 800$ ms, $TE = 29$ ms, flip-angle = 60° , matrix size = 64×64 , voxel size = $3 \times 3 \times 3$ mm 3 , 42 axial slices with interleaved acquisition, no slice gap). Single-band reference images were also collected in both resting-state acquisitions for head motion realignment. During both acquisitions, participants were instructed to keep their eyes open, fixating a white cross that they saw through a mirror located on the head coil, and not to think about anything specific. Field maps were also obtained to correct for field distortions.

3.2. Selection of the hemodynamic response function

With the aim of making a fair comparison of the two methods, we first compared their hemodynamic response functions. Figure 3A shows the difference in the hemodynamic response function that PFM and TA use by default for $TR = 0.1$ s and $TR = 1$ s adjusted to peak amplitude of one; i.e., the canonical HRF and the HRF resulting from the linear differential operator. The most observable difference between the two HRFs is the time to peak: the HRF used by Total Activation does not begin at zero while the one used by PFM does.

While Paradigm Free Mapping allows for the use of any hemodynamic response function — the columns of the design matrix \mathbf{H} are composed by shifted versions of the HRF—the linear differential operator in TA is tailored for a fixed HRF. Hence, for practical reasons, we reproduced the HRF in the Total Activation filter and incorporated it into the PFM formulation (Figure 3B).

3.3. Selection of the regularization parameter based on the estimation of the noise

Total Activation proposes to solve the inverse problem by updating the regularization parameter λ on every iteration n so that the residuals converge to a previously estimated noise level of the data fit $\tilde{\sigma}$, where this pre-estimated noise is calculated from the median absolute deviation of

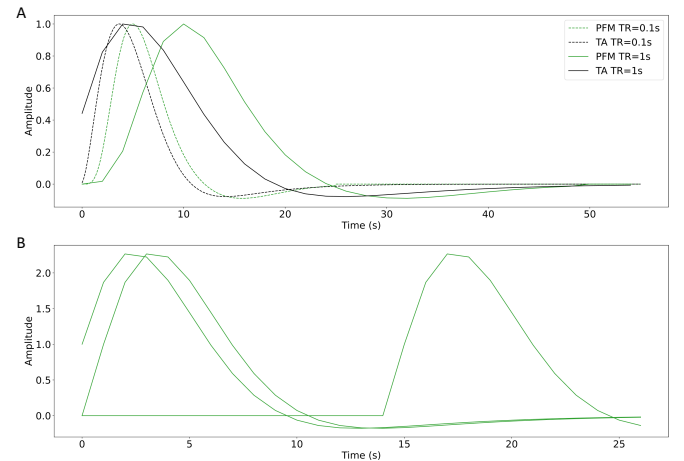


Figure 3: A) Canonical HRF models typically used by PFM (green) and TA (black) at $TR = 0.1$ s (dashed lines) and $TR = 1$ s (solid lines). Without loss of generality, the waveforms are scaled to unit amplitude for visualization. B) Representation of three shifted HRFs at $TR=1$ s (onsets=0, 1, and 15 s) that build the design matrix for PFM when the HRF model has been matched to that in TA.

fine-scale wavelet coefficients (Daubechies, order 3) (Karanoglu et al. 2013):

$$\lambda^{n+1} = \frac{N\tilde{\sigma}}{\frac{1}{2}\|\mathbf{y} - \mathbf{x}^n\|_F^2}\lambda^n. \quad (10)$$

Thus, we calculated the regularization path with PFM (as described in 3.4) and selected the λ corresponding to the residuals that were closest to the estimated noise level of the data. We applied Total Activation with temporal regularization in its original form. Figure 4 depicts the estimated activity-inducing, innovation, and activity-related signals when updating λ as in (10) in the three simulated SNR settings using the spike model (left) and the block model (right). Figure 4 (left) shows nearly identical results between PFM (left) and TA (right) with the use of the spike model. The minimal differences are the result of slight dissimilarities in the convergence of the residuals to the estimated noise level of the data. Likewise, the use of the block model with a selection of λ based on the MAD estimate of the noise yields results that are identical in practice as shown in Figure 4 (right).

In addition, we performed the same comparison on experimental data as introduced in 3.1. Figure 5 (row 3) illustrates that the estimated activity-inducing, innovation, and activity-related signals with PFM and TA are practically identical both for the spike model (left) and the block model (right).

3.4. Selection of the regularization parameter by solving the regularization path

Paradigm Free Mapping bases its selection of the regularization parameter on the Bayesian Information Criterion (BIC) and the Akaike Information Criterion (AIC). Hence, we calculated the regularization path with PFM

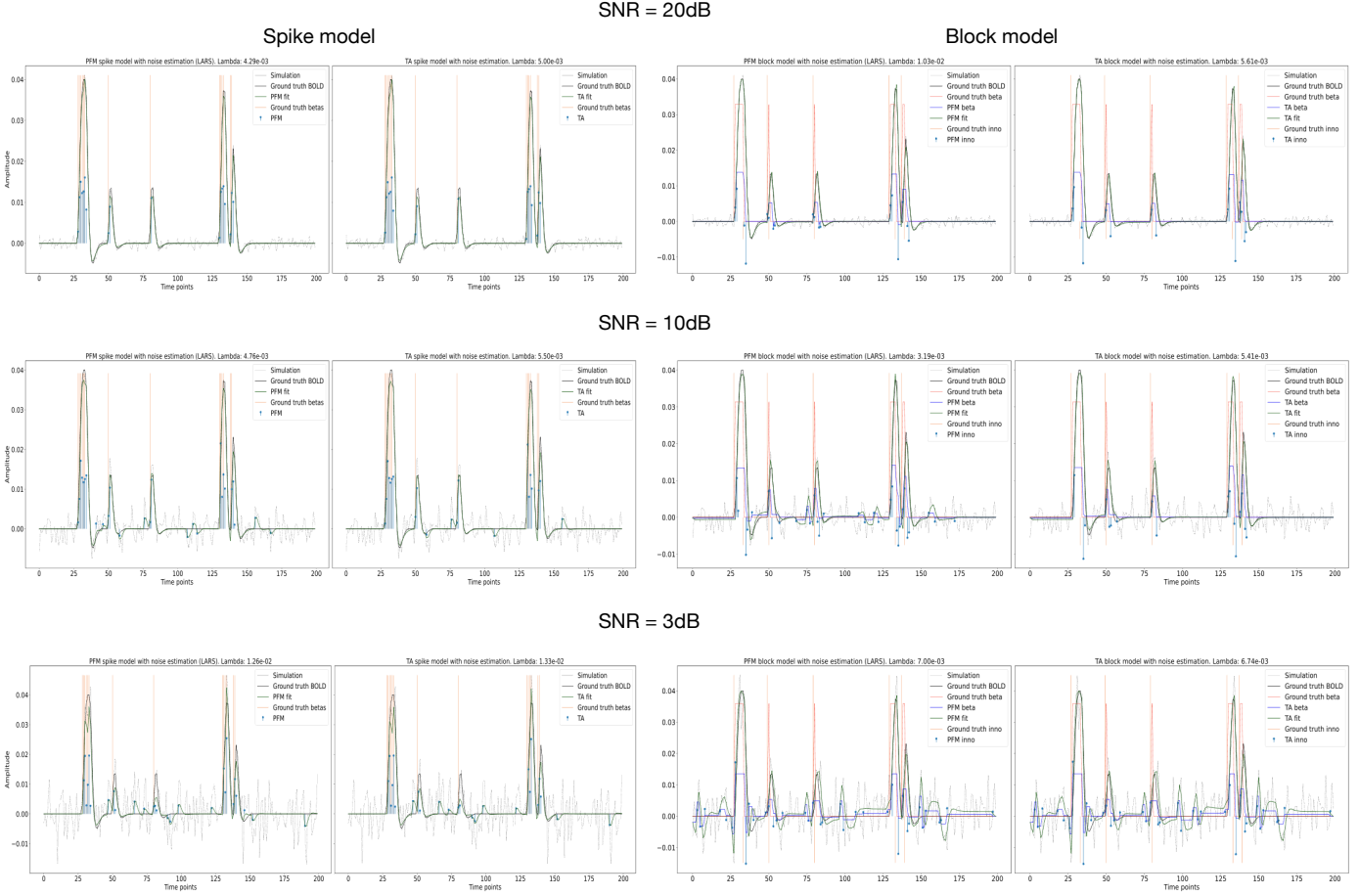


Figure 4: Estimated activity-inducing, innovation and activity-related (fit, \mathbf{x}) signals when λ is selected based on convergence of residuals to have same variance as MAD estimate of noise with spike model (left, with PFM on the left and TA on the right) and block model (right, with PFM on the left and TA on the right) on SNR = 20 dB (top), SNR = 10 dB (middle) and SNR = 3 dB (bottom).

240 by means of the least angle regression (LARS) algorithm (Efron et al. 2004) and used the λ s from the regularization 245 path to solve the deconvolution problem with Total Activation.

Figure 6 (left) shows the regularization paths of PFM₂₆₅ and TA side by side for the three SNR conditions for the spike model; i.e., the inverse problem described in (3). Each iteration of LARS reduces the value of λ ; i.e., reduces the sparsity promoted by the l_1 -norm, and reveals new non-zero coefficients as shown in the x axis of the₂₇₀ heatmaps. Vertical black lines depict the selection of the regularization parameter based on BIC and AIC, and thus, the colored coefficients indicated by the vertical lines depict the estimated activity-inducing signal $s(t)$. Figure 6 (right) illustrates the resulting estimation of the activity-₂₇₅ inducing and neuronal-related signals when basing the selection of λ on BIC for the three simulated SNR conditions. Given that the regularization paths of both techniques are identical, the BIC-based selection of the regularization parameter and the results of deconvolving with₂₈₀ said λ are identical too (see Figure ??). Thus, Figure 6

demonstrates that, regardless of the simulated SNR condition, both deconvolution algorithms produce identical regularization paths when the same HRF and regularization parameters are applied, and hence, identical estimates of the activity-inducing signal s and neuronal-related signal \mathbf{x} .

The regularization path to estimate innovation signals yields mainly undistinguishable results for both PFM and TA methods as shown in Figure 7 (left). Again, the BIC-based selection of λ is identical for both PFM and TA, and the estimation of the innovation signal \mathbf{u} shows no distinguishable differences between the algorithms (see Figure 7 right). Therefore, both Paradigm Free Mapping and Total Activation yield nearly identical regularization paths and estimates of the innovation signal regardless of the simulated SNR condition when applying the same HRF and regularization parameters with the block model.

Furthermore, we performed the same analysis on experimental data as shown in Figure 5 (rows 1-2, 4). Row 1 demonstrates that the PFM and TA regularization paths are identical when deconvolving experimental data, re-

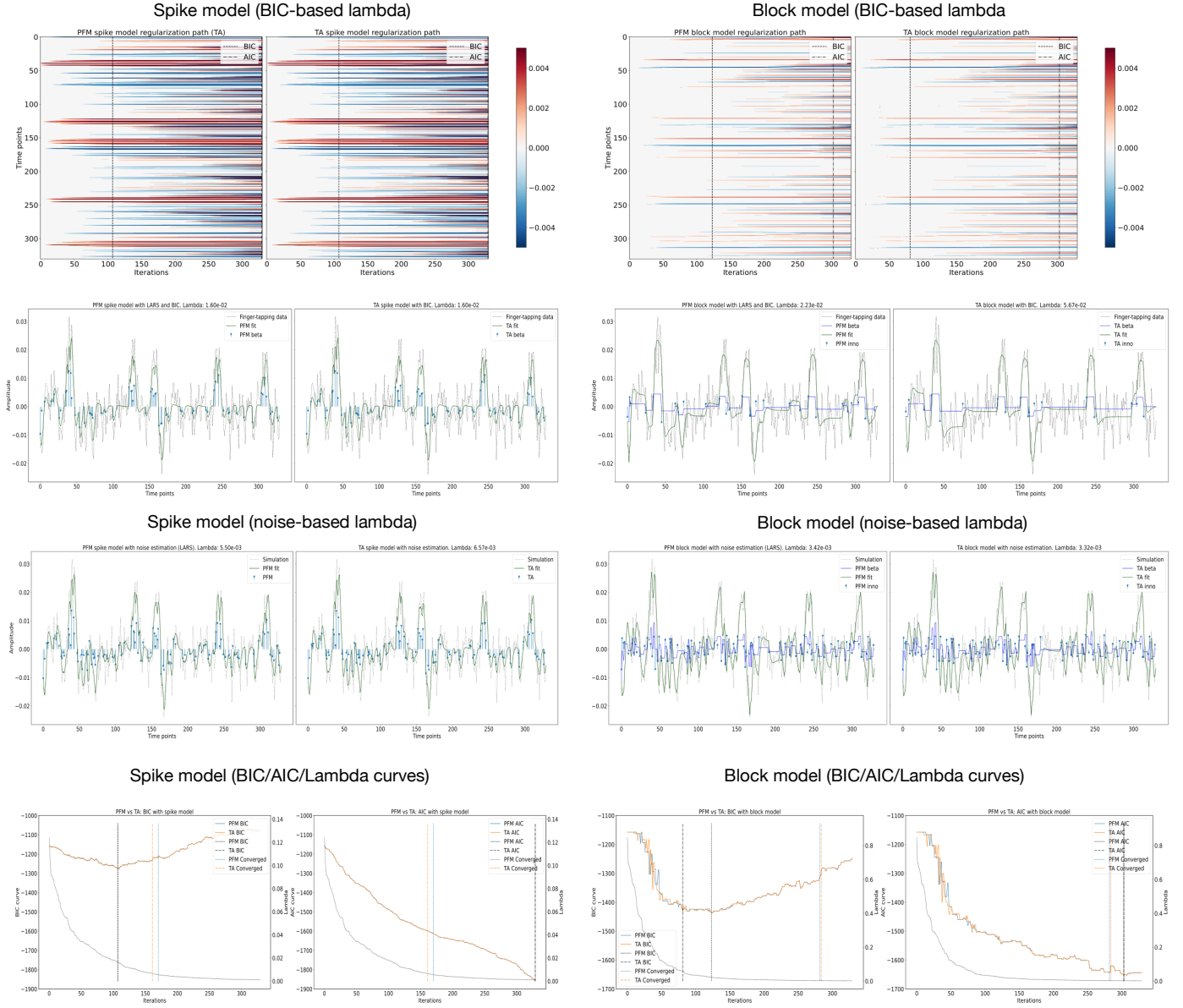


Figure 5: (Row 1) Regularization paths of the estimated activity-inducing signal (spike model — left) and innovation signal (block model — right); (Row 2) activity-inducing, innovation and activity-related (fit, \mathbf{x}) signals when λ is selected based on BIC, or (Row 3) based on convergence of residuals to have same variance as MAD estimate of noise; (Row 4) Corresponding cost curves of BIC and AIC. The vertical lines indicate the three options to select λ (BIC, AIC and Converged/MAD).

285
290
295
300
305
310
315
320
325
330
335
340
345
350
355
360
365
370
375
380
385
390
395
400
405
410
415
420
425
430
435
440
445
450
455
460
465
470
475
480
485
490
495
500
505
510
515
520
525
530
535
540
545
550
555
560
565
570
575
580
585
590
595
600
605
610
615
620
625
630
635
640
645
650
655
660
665
670
675
680
685
690
695
700
705
710
715
720
725
730
735
740
745
750
755
760
765
770
775
780
785
790
795
800
805
810
815
820
825
830
835
840
845
850
855
860
865
870
875
880
885
890
895
900
905
910
915
920
925
930
935
940
945
950
955
960
965
970
975
980
985
990
995
1000
1005
1010
1015
1020
1025
1030
1035
1040
1045
1050
1055
1060
1065
1070
1075
1080
1085
1090
1095
1100
1105
1110
1115
1120
1125
1130
1135
1140
1145
1150
1155
1160
1165
1170
1175
1180
1185
1190
1195
1200
1205
1210
1215
1220
1225
1230
1235
1240
1245
1250
1255
1260
1265
1270
1275
1280
1285
1290
1295
1300
1305
1310
1315
1320
1325
1330
1335
1340
1345
1350
1355
1360
1365
1370
1375
1380
1385
1390
1395
1400
1405
1410
1415
1420
1425
1430
1435
1440
1445
1450
1455
1460
1465
1470
1475
1480
1485
1490
1495
1500
1505
1510
1515
1520
1525
1530
1535
1540
1545
1550
1555
1560
1565
1570
1575
1580
1585
1590
1595
1600
1605
1610
1615
1620
1625
1630
1635
1640
1645
1650
1655
1660
1665
1670
1675
1680
1685
1690
1695
1700
1705
1710
1715
1720
1725
1730
1735
1740
1745
1750
1755
1760
1765
1770
1775
1780
1785
1790
1795
1800
1805
1810
1815
1820
1825
1830
1835
1840
1845
1850
1855
1860
1865
1870
1875
1880
1885
1890
1895
1900
1905
1910
1915
1920
1925
1930
1935
1940
1945
1950
1955
1960
1965
1970
1975
1980
1985
1990
1995
2000
2005
2010
2015
2020
2025
2030
2035
2040
2045
2050
2055
2060
2065
2070
2075
2080
2085
2090
2095
2100
2105
2110
2115
2120
2125
2130
2135
2140
2145
2150
2155
2160
2165
2170
2175
2180
2185
2190
2195
2200
2205
2210
2215
2220
2225
2230
2235
2240
2245
2250
2255
2260
2265
2270
2275
2280
2285
2290
2295
2300
2305
2310
2315
2320
2325
2330
2335
2340
2345
2350
2355
2360
2365
2370
2375
2380
2385
2390
2395
2400
2405
2410
2415
2420
2425
2430
2435
2440
2445
2450
2455
2460
2465
2470
2475
2480
2485
2490
2495
2500
2505
2510
2515
2520
2525
2530
2535
2540
2545
2550
2555
2560
2565
2570
2575
2580
2585
2590
2595
2600
2605
2610
2615
2620
2625
2630
2635
2640
2645
2650
2655
2660
2665
2670
2675
2680
2685
2690
2695
2700
2705
2710
2715
2720
2725
2730
2735
2740
2745
2750
2755
2760
2765
2770
2775
2780
2785
2790
2795
2800
2805
2810
2815
2820
2825
2830
2835
2840
2845
2850
2855
2860
2865
2870
2875
2880
2885
2890
2895
2900
2905
2910
2915
2920
2925
2930
2935
2940
2945
2950
2955
2960
2965
2970
2975
2980
2985
2990
2995
3000
3005
3010
3015
3020
3025
3030
3035
3040
3045
3050
3055
3060
3065
3070
3075
3080
3085
3090
3095
3100
3105
3110
3115
3120
3125
3130
3135
3140
3145
3150
3155
3160
3165
3170
3175
3180
3185
3190
3195
3200
3205
3210
3215
3220
3225
3230
3235
3240
3245
3250
3255
3260
3265
3270
3275
3280
3285
3290
3295
3300
3305
3310
3315
3320
3325
3330
3335
3340
3345
3350
3355
3360
3365
3370
3375
3380
3385
3390
3395
3400
3405
3410
3415
3420
3425
3430
3435
3440
3445
3450
3455
3460
3465
3470
3475
3480
3485
3490
3495
3500
3505
3510
3515
3520
3525
3530
3535
3540
3545
3550
3555
3560
3565
3570
3575
3580
3585
3590
3595
3600
3605
3610
3615
3620
3625
3630
3635
3640
3645
3650
3655
3660
3665
3670
3675
3680
3685
3690
3695
3700
3705
3710
3715
3720
3725
3730
3735
3740
3745
3750
3755
3760
3765
3770
3775
3780
3785
3790
3795
3800
3805
3810
3815
3820
3825
3830
3835
3840
3845
3850
3855
3860
3865
3870
3875
3880
3885
3890
3895
3900
3905
3910
3915
3920
3925
3930
3935
3940
3945
3950
3955
3960
3965
3970
3975
3980
3985
3990
3995
4000
4005
4010
4015
4020
4025
4030
4035
4040
4045
4050
4055
4060
4065
4070
4075
4080
4085
4090
4095
4100
4105
4110
4115
4120
4125
4130
4135
4140
4145
4150
4155
4160
4165
4170
4175
4180
4185
4190
4195
4200
4205
4210
4215
4220
4225
4230
4235
4240
4245
4250
4255
4260
4265
4270
4275
4280
4285
4290
4295
4300
4305
4310
4315
4320
4325
4330
4335
4340
4345
4350
4355
4360
4365
4370
4375
4380
4385
4390
4395
4400
4405
4410
4415
4420
4425
4430
4435
4440
4445
4450
4455
4460
4465
4470
4475
4480
4485
4490
4495
4500
4505
4510
4515
4520
4525
4530
4535
4540
4545
4550
4555
4560
4565
4570
4575
4580
4585
4590
4595
4600
4605
4610
4615
4620
4625
4630
4635
4640
4645
4650
4655
4660
4665
4670
4675
4680
4685
4690
4695
4700
4705
4710
4715
4720
4725
4730
4735
4740
4745
4750
4755
4760
4765
4770
4775
4780
4785
4790
4795
4800
4805
4810
4815
4820
4825
4830
4835
4840
4845
4850
4855
4860
4865
4870
4875
4880
4885
4890
4895
4900
4905
4910
4915
4920
4925
4930
4935
4940
4945
4950
4955
4960
4965
4970
4975
4980
4985
4990
4995
5000
5005
5010
5015
5020
5025
5030
5035
5040
5045
5050
5055
5060
5065
5070
5075
5080
5085
5090
5095
5100
5105
5110
5115
5120
5125
5130
5135
5140
5145
5150
5155
5160
5165
5170
5175
5180
5185
5190
5195
5200
5205
5210
5215
5220
5225
5230
5235
5240
5245
5250
5255
5260
5265
5270
5275
5280
5285
5290
5295
5300
5305
5310
5315
5320
5325
5330
5335
5340
5345
5350
5355
5360
5365
5370
5375
5380
5385
5390
5395
5400
5405
5410
5415
5420
5425
5430
5435
5440
5445
5450
5455
5460
5465
5470
5475
5480
5485
5490
5495
5500
5505
5510
5515
5520
5525
5530
5535
5540
5545
5550
5555
5560
5565
5570
5575
5580
5585
5590
5595
5600
5605
5610
5615
5620
5625
5630
5635
5640
5645
5650
5655
5660
5665
5670
5675
5680
5685
5690
5695
5700
5705
5710
5715
5720
5725
5730
5735
5740
5745
5750
5755
5760
5765
5770
5775
5780
5785
5790
5795
5800
5805
5810
5815
5820
5825
5830
5835
5840
5845
5850
5855
5860
5865
5870
5875
5880
5885
5890
5895
5900
5905
5910
5915
5920
5925
5930
5935
5940
5945
5950
5955
5960
5965
5970
5975
5980
5985
5990
5995
6000
6005
6010
6015
6020
6025
6030
6035
6040
6045
6050
6055
6060
6065
6070
6075
6080
6085
6090
6095
6100
6105
6110
6115
6120
6125
6130
6135
6140
6145
6150
6155
6160
6165
6170
6175
6180
6185
6190
6195
6200
6205
6210
6215
6220
6225
6230
6235
6240
6245
6250
6255
6260
6265
6270
6275
6280
6285
6290
6295
6300
6305
6310
6315
6320
6325
6330
6335
6340
6345
6350
6355
6360
6365
6370
6375
6380
6385
6390
6395
6400
6405
6410
6415
6420
6425
6430
6435
6440
6445
6450
6455
6460
6465
6470
6475
6480
6485
6490
6495
6500
6505
6510
6515
6520
6525
6530
6535
6540
6545
6550
6555
6560
6565
6570
6575
6580
6585
6590
6595
6600
6605
6610
6615
6620
6625
6630
6635
6640
6645
6650
6655
6660
6665
6670
6675
6680
6685
6690
6695
6700
6705
6710
6715
6720
6725
6730
6735
6740
6745
6750
6755
6760
6765
6770
6775
6780
6785
6790
6795
6800
6805
6810
6815
6820
6825
6830
6835
6840
6845
6850
6855
6860
6865
6870
6875
6880
6885
6890
6895
6900
6905
6910
6915
6920
6925
6930
6935
6940
6945
6950
6955
6960
6965
6970
6975
6980
6985
6990
6995
7000
7005
7010
7015
7020
7025
7030
7035
7040
7045
7050
7055
7060
7065
7070
7075
7080
7085
7090
7095
7100
7105
7110
7115
7120
7125
7130
7135
7140
7145
7150
7155
7160
7165
7170
7175
7180
7185
7190
7195
7200
7205
7210
7215
7220
7225
7230
7235
7240
7245
7250
7255
7260
7265
7270
7275
7280
7285
7290
7295
7300
7305
7310
7315
7320
7325
7330
7335
7340
7345
7350
7355
7360
7365
7370
7375
7380
7385
7390
7395
7400
7405
7410
7415
7420
7425
7430
7435
7440
7445
7450
7455
7460
7465
7470
7475
7480
7485
7490
7495
7500
7505
7510
7515
7520
7525
7530
7535
7540
7545
7550
7555
7560
7565
7570
7575
7580
7585
7590
7595
7600
7605
7610
7615
7620
7625
7630
7635
7640
7645
7650
7655
7660
7665
7670
7675
7680
7685
7690
7695
7700
7705
7710
7715
7720
7725
7730
7735
7740
7745
7750
7755
7760
7765
7770
7775
7780
7785
7790
7795
7800
7805
7810
7815
7820
7825
7830
7835
7840
7845
7850
7855
7860
7865
7870
7875
7880
7885
7890
7895
7900
7905
7910
7915
7920
7925
7930
7935
7940
7945
7950
7955
7960
7965
7970
7975
7980
7985
7990
7995
8000
8005
8010
8015
8020
8025
8030
8035
8040
8045
8050
8055
8060
8065
8070
8075
8080
8085
8090
8095
8100
8105
8110
8115
8120
8125
8130
8135
8140
8145
8150
8155
8160
8165
8170
8175
8180
8185
8190
8195
8200
8205
8210
8215
8220
8225
8230
8235
8240
8245
8250
8255
8260
8265
8270
8275
8280
8285
8290
8295
8300
8305
8310
8315
8320
8325
8330
8335
8340
8345
8350
8355
8360
8365
8370
8375
8380
8385
8390
8395
8400
8405
8410
8415
8420
8425
8430
8435
8440
8445
8450
8455
8460
8465
8470
8475
8480
8485
8490
8495
8500
8505
8510
8515
8520
8525
8530
8535
8540
8545
8550
8555
8560
8565
8570
8575
8580
8585
8590
8595
8600
8605
8610
8615
8620
8625
8630
8635
8640
8645
8650
8655
8660
8665
8670
8675
8680
8685
8690
8695
8700
8705
8710
8715
8720
8725
8730
8735
8740
8745
8750
8755
8760
8765
8770
8775
8780
8785
8790
8795
8800
8805
8810
8815
8820
8825
8830
8835
8840
8845
8850
8855
8860
8865
8870
8875
8880
8885
8890
8895
8900
8905
8910
8915
8920
8925
8930
8935
8940
8945
8950
8955
8960
8965
8970
8975
898

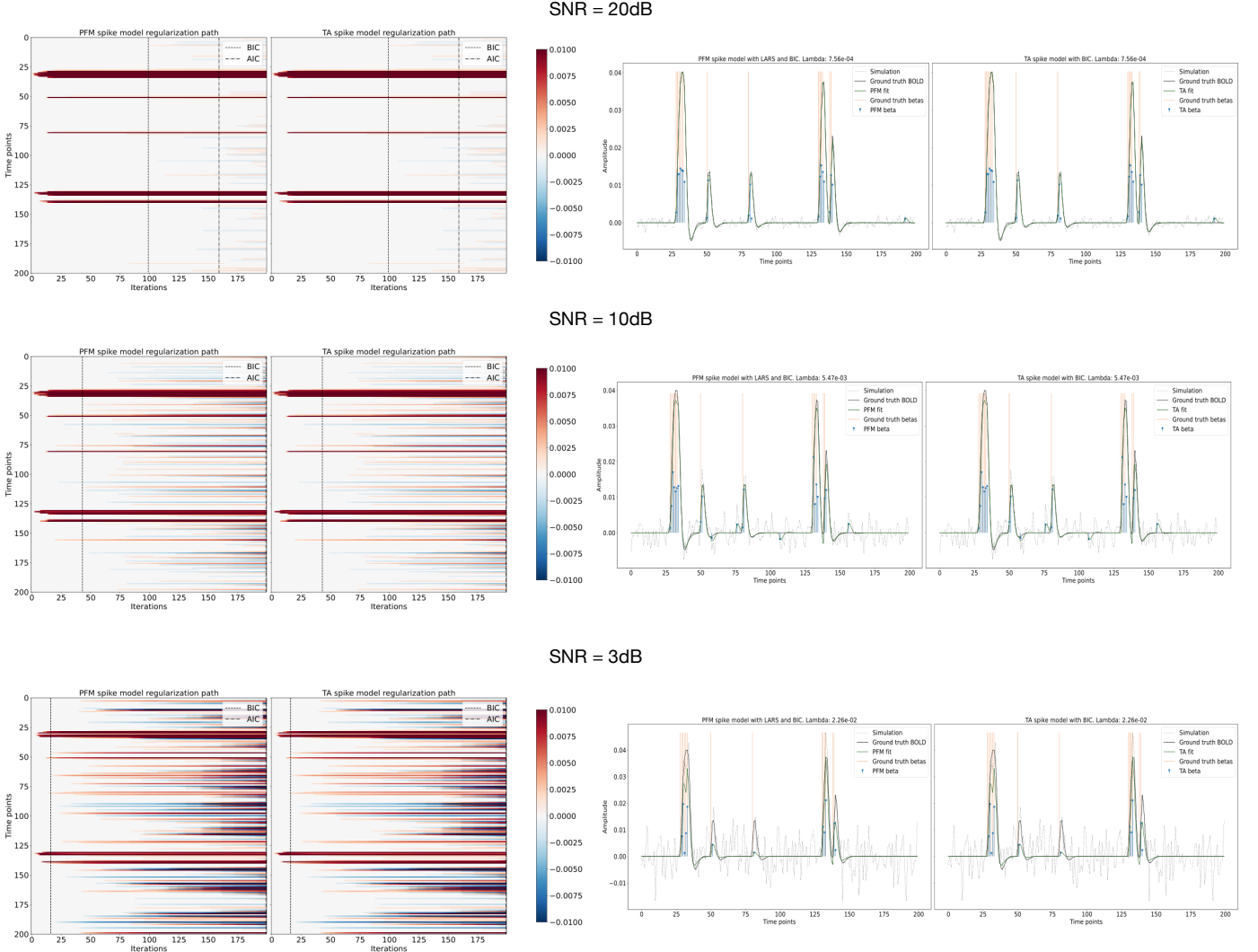


Figure 6: Spike model simulations. (Left) Heatmap of the regularization paths of the activity-inducing signal estimated with PFM and TA as a function of λ (increasing number of iterations in x-axis), whereas each row in the y-axis shows one time-point. Vertical lines denote iterations corresponding to the Akaike and Bayesian Information Criteria (AIC and BIC) optima. (Right) Estimated activity-inducing (blue) and activity-related (green) signals when set based on BIC. All estimates are identical, regardless of SNR.

4. Discussion

This work demonstrates that Paradigm Free Mapping and Total Activation yield practically identical results when the same HRF model and regularization parameter are employed, demonstrating that synthesis and analysis models are equivalent for temporal fMRI deconvolution. Thus, previously observed differences in performance must be due to differences in usage options. With the equivalence in the temporal deconvolution demonstrated, it is reasonable to assume that additional regularization terms in the spatial or temporal domains would not modify this equivalence when convex operators are employed; e.g., when the regularization problem can be solved by means of the Fast Iterative Shrinkage-Thresholding Algorithm (FISTA) (Beck and Teboulle 2009) or the Generalized Forward-

Backward Splitting (Raguet et al. 2013) techniques. Our findings are in line with the equivalence of analysis and synthesis methods in under-determined cases ($N \leq V$) as demonstrated in (Elad et al. 2007).

Taking into account the advantages and disadvantages of the presented techniques shown in Table 1, future work will improve and extend deconvolution methods for fMRI. For instance, the appropriate formulation depending on data acquisition (i.e., single-echo vs multi-echo) could be studied and compared with existing methods (Caballero-Gaudes et al. 2019), or formulations that account for HRF variability could be investigated too (Badillo et al. 2013; Gaudes et al. 2012; Farouj et al. 2019). Furthermore, robust methods to select the regularization parameter (Uruñuela et al. 2020; Meinshausen and Bühlmann 2010) and other

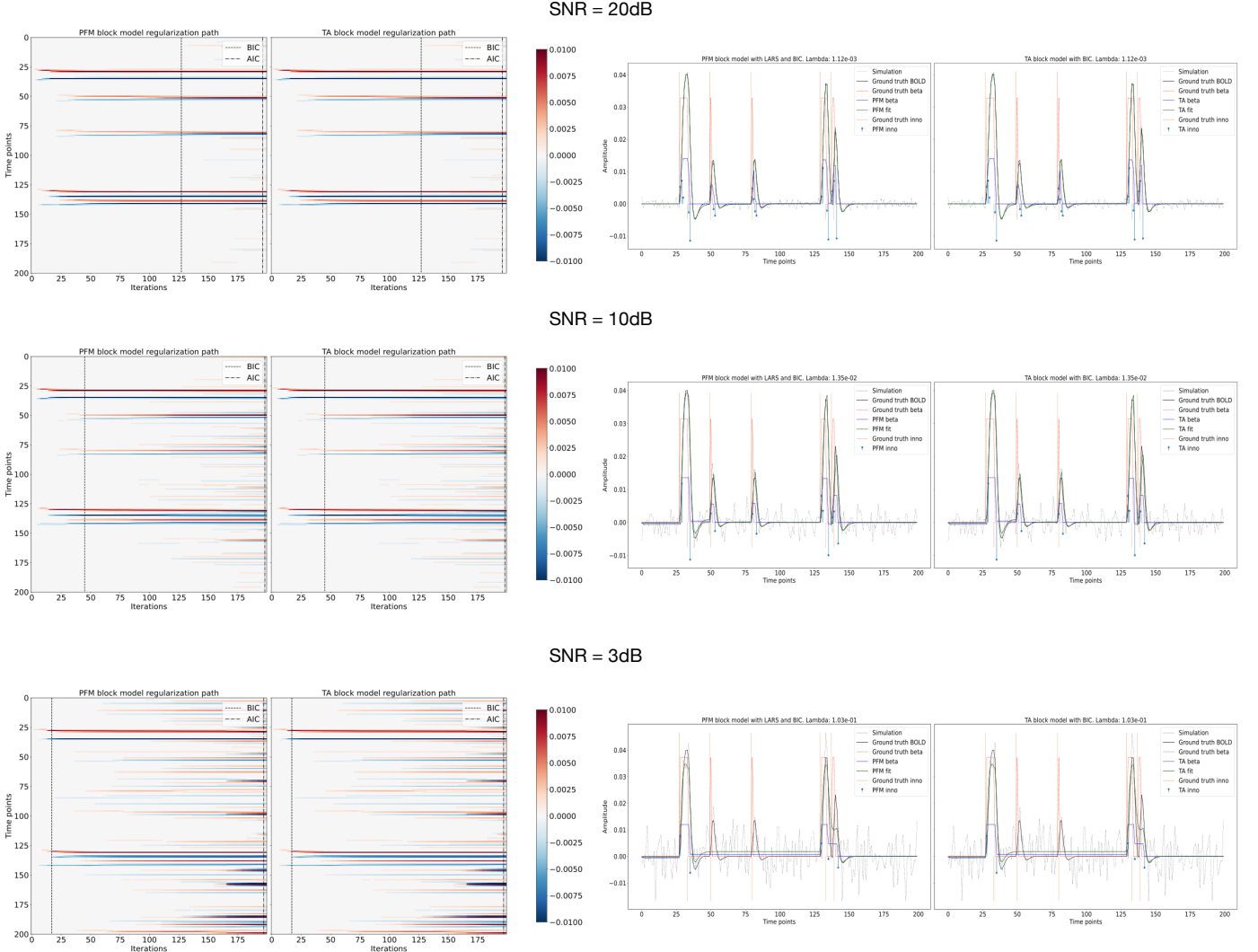


Figure 7: Block model simulations. (Left) Heatmap of the regularization paths of the innovation signal estimated with PFM and TA as a function of λ (increasing number of iterations in x-axis), whereas each row in the y-axis illustrates one time-point. Vertical lines denote iterations corresponding to the Akaike and Bayesian Information Criteria (AIC and BIC) optima. (Right) Estimated innovation (blue) and activity-related (green) signals when λ is set based on BIC. All the estimates are identical when compared between the PFM and TA cases, regardless of SNR.

potential $\ell_{p,q}$ -norm regularization terms (e.g., $p < 1$) or debiasing approaches could be explored.

325

5. Code availability

The code and materials used in this work can be found in the following GitHub repository: https://github.com/eurunuela/pfm_vs_ta. We encourage the reader to play with the parameters (e.g. SNR, varying HRF options and mismatch between algorithms, TR, number of events, onsets, and durations) in the provided Jupyter notebooks.

330

6. Acknowledgements

This research was funded by the European Union's Horizon 2020 research and innovation program (agreement No. 713673 of the Marie Skłodowska-Curie grant), La Caixa Foundation (ID 100010434, fellowship code LCF/B Q/IN17/11620063), the Spanish Ministry of Economy and Competitiveness (RYC-2017-21845), the Basque Government (BERC 2018-2021, PIBA_2019_104, PRE_2019_1_0054), and the Spanish Ministry of Science, Innovation and Universities (PID2019-105520GB-100).

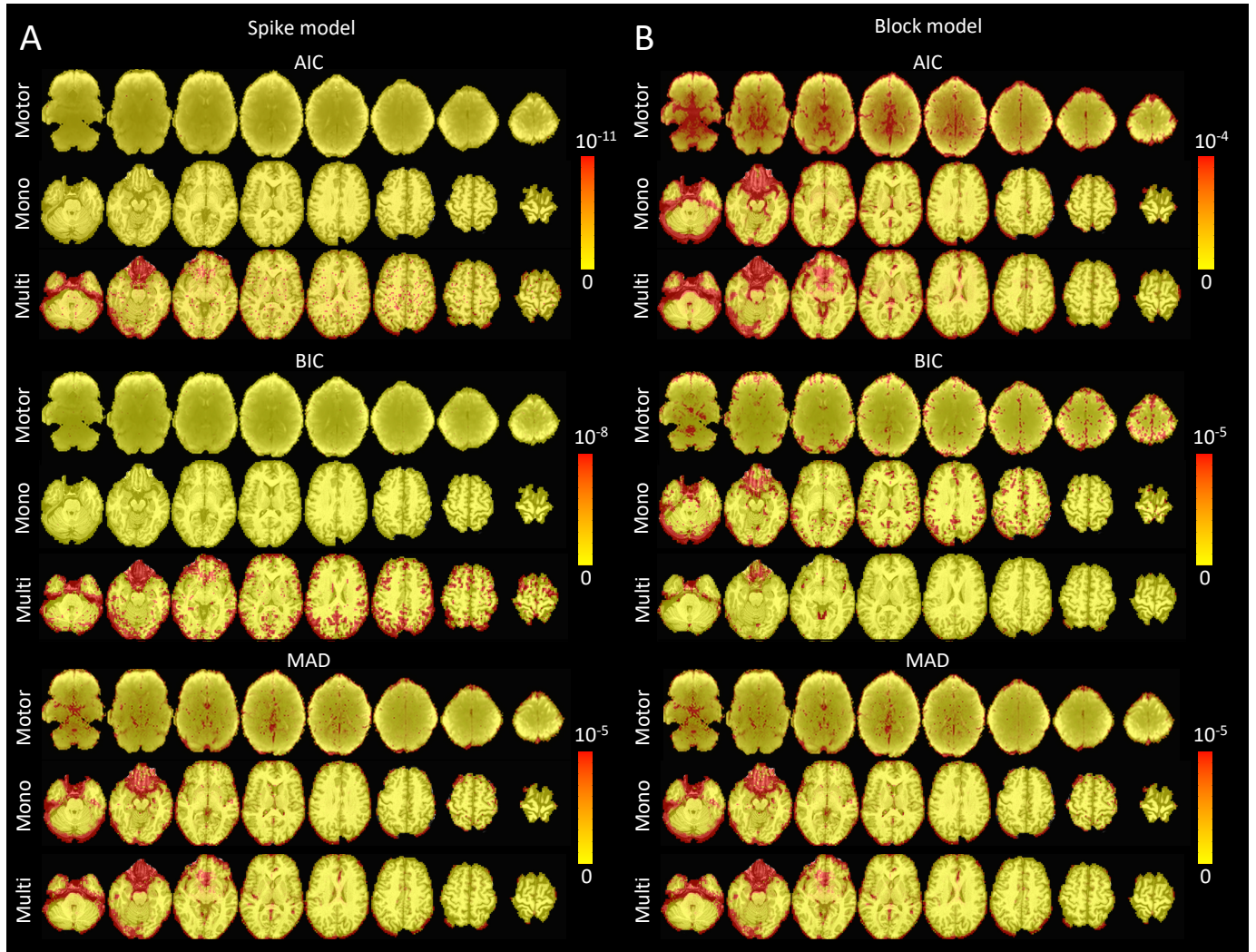


Figure 8: Sum of squares of the differences of the activity-inducing signals estimated with Paradigm Free Mapping and Total activation for the different selections of the regularization parameter: AIC (top), BIC (middle), and MAD (bottom). The sum of square difference maps are shown for the three experimental datasets introduced in Section 3.1: the motor task (Motor), the monoband resting-state (Mono), and the multiband resting-state (Multi) datasets. A) Sum of squares of the differences when using the spike model. B) Sum of squares of the differences when using the block model.

References

- Akaike, H., 1998. Information Theory and an Extension of the Maximum Likelihood Principle, in: Parzen, E., Tanabe, K., Kitagawa, G. (Eds.), Selected Papers of Hirotugu Akaike. Springer, New York, NY. Springer Series in Statistics, pp. 199–213. doi:10.1007/978-1-4612-1694-0_15.
- Allan, T.W., Francis, S.T., Caballero-Gaudes, C., Morris, P.G., Liddle, E.B., Liddle, P.F., Brookes, M.J., Gowland, P.A., 2015. Functional connectivity in mri is driven by spontaneous bold events. *PloS one* 10, e0124577.
- Badillo, S., Vincent, T., Ciuciuc, P., 2013. Group-level impacts of within-and between-subject hemodynamic variability in fmri. *Neuroimage* 82, 433–448.
- Beck, A., Teboulle, M., 2009. A fast iterative shrinkage-thresholding algorithm. *Society for Industrial and Applied Mathematics Journal on Imaging Sciences* 2, 183–202. doi:10.1137/080716542.
- Betzel, R.F., Byrge, L., Esfahlani, F.Z., Kennedy, D.P., 2020. Temporal fluctuations in the brain's modular architecture during movie-watching. *NeuroImage* 213, 116687. doi:10.1016/j.neuroimage.2020.116687.
- Bommarito, G., Tarun, A., Farouj, Y., Preti, M.G., Petracca, M., Droby, A., El Mendili, M.M., Inglese, M., Van De Ville, D., 2020. Functional network dynamics in progressive multiple sclerosis. *medRxiv*.
- Bruckstein, A.M., Donoho, D.L., Elad, M., 2009. From Sparse Solutions of Systems of Equations to Sparse Modeling of Signals and Images. *SIAM Review* 51, 34–81. doi:10.1137/060657704.
- Caballero-Gaudes, C., Moia, S., Panwar, P., Bandettini, P.A., Gonzalez-Castillo, J., 2019. A deconvolution algorithm for multi-echo functional mri: Multi-echo sparse paradigm free mapping. *NeuroImage* 202, 116081.
- Caballero Gaudes, C., Petridou, N., Francis, S.T., Dryden, I.L., Gowland, P.A., 2013. Paradigm free mapping with sparse regression automatically detects single-trial functional magnetic resonance imaging blood oxygenation level dependent responses. *Human Brain Mapping* doi:10.1002/hbm.21452.
- Cherkaoui, H., Moreau, T., Halimi, A., Ciuciuc, P., 2019. Sparsity-based Blind Deconvolution of Neural Activation Signal in FMRI, in: ICASSP 2019 - 2019 IEEE International Conference on Acoustics, Speech and Signal Processing (ICASSP), pp. 1323–1327.

Paradigm Free Mapping	Total Activation
+ Its formulation can be extended straightforwardly for deconvolution of multiple signals with a common neuronal-related signal, e.g., for multi-echo formulations Caballero-Gaudes et al. 2019.	420
+ Both the spike and block models solve the regularization problem with the same HRF.	425
+ The model can implement any HRF shape very easily since it only requires the coefficients at the required temporal resolution.	430
-	435
	440
	445
	450
	455
	460
	465
	470
	475
	480
	485
	490
	495
	500
	505
	510
	515
	520
	525
	530
	535
	540
	545
	550
	555
	560
	565
	570
	575
	580
	585
	590
	595
	600
	605
	610
	615
	620
	625
	630
	635
	640
	645
	650
	655
	660
	665
	670
	675
	680
	685
	690
	695
	700
	705
	710
	715
	720
	725
	730
	735
	740
	745
	750
	755
	760
	765
	770
	775
	780
	785
	790
	795
	800
	805
	810
	815
	820
	825
	830
	835
	840
	845
	850
	855
	860
	865
	870
	875
	880
	885
	890
	895
	900
	905
	910
	915
	920
	925
	930
	935
	940
	945
	950
	955
	960
	965
	970
	975
	980
	985
	990
	995
	1000

Table 1: Advantages (+) and disadvantages (-) of Paradigm Free Mapping and Total Activation with respect to each other.

doi:10.1109/ICASSP.2019.8683358.

- Efron, B., Hastie, T., Johnstone, I., Tibshirani, R., 2004. Least Angle Regression. *The Annals of Statistics* 32, 407–499. doi:10.1214/009053604000000067.
- Elad, M., Milanfar, P., Rubinstein, R., 2007. Analysis versus synthesis in signal priors. *Inverse problems* 23, 947.
- Esfahlani, F.Z., Jo, Y., Faskowitz, J., Byrge, L., Kennedy, D.P., Sporns, O., Betzel, R.F., 2020. High-amplitude cofluctuations in cortical activity drive functional connectivity. *Proceedings of the National Academy of Sciences* 117, 28393–28401.
- Farouj, Y., Karahanoglu, F.I., Van De Ville, D., 2019. Bold signal deconvolution under uncertain haemodynamics: A semi-blind approach, in: 2019 IEEE 16th International Symposium on Biomedical Imaging (ISBI 2019), IEEE. pp. 1792–1796.
- Faskowitz, J., Esfahlani, F.Z., Jo, Y., Sporns, O., Betzel, R.F., 2020. Edge-centric functional network representations of human cerebral cortex reveal overlapping system-level architecture. *Technical Report*. Nature Publishing Group.
- Finn, E.S., Bandettini, P.A., 2020. Movie-watching outperforms rest for functional connectivity-based prediction of behavior. *bioRxiv*, 2020.08.23.263723–2020.08.23.263723doi:10.1101/2020.08.23.263723.
- Finn, E.S., Gleean, E., Khojandi, A.Y., Nielson, D., Molfese, P.J., Handwerker, D.A., Bandettini, P.A., 2020. Idiosynchrony: From shared responses to individual differences during naturalistic neuroimaging. *NeuroImage* 215, 116828–116828. doi:10.1016/j.neuroimage.2020.116828.
- Gaudes, C.C., Karahanoglu, F.I., Lazeyras, F., Van De Ville, D., 2012. Structured sparse deconvolution for paradigm free mapping of functional mri data, in: 2012 9th IEEE International Symposium on Biomedical Imaging (ISBI), IEEE. pp. 322–325.
- Gaudes, C.C., Petridou, N., Dryden, I.L., Bai, L., Francis, S.T., Gowland, P.A., 2011. Detection and characterization of single-trial fMRI bold responses: Paradigm free mapping. *Human Brain Mapping* doi:10.1002/hbm.21116.

- Gitelman, D.R., Penny, W.D., Ashburner, J., Friston, K.J., 2003. Modeling regional and psychophysiological interactions in fMRI: The importance of hemodynamic deconvolution. *NeuroImage* 19, 200–207. doi:10.1016/S1053-8119(03)00058-2.
- Gonzalez-Castillo, J., Caballero-Gaudes, C., Topolski, N., Handwerker, D.A., Pereira, F., Bandettini, P.A., 2019. Imaging the spontaneous flow of thought: Distinct periods of cognition contribute to dynamic functional connectivity during rest. *NeuroImage* 202, 116129. doi:10.1016/j.neuroimage.2019.116129.
- Karahanoglu, F.I., Bayram, I., Ville, D.V.D., 2011. A Signal Processing Approach to Generalized 1-D Total Variation. *IEEE Transactions on Signal Processing* 59, 5265–5274. doi:10.1109/TSP.2011.2164399.
- Karahanoglu, F.I., Caballero-Gaudes, C., Lazeyras, F., Van De Ville, D., 2013. Total activation: FMRI deconvolution through spatio-temporal regularization. *NeuroImage* doi:10.1016/j.neuroimage.2013.01.067.
- Karahanoglu, F.I., Van De Ville, D., 2015. Transient brain activity disentangles fMRI resting-state dynamics in terms of spatially and temporally overlapping networks. *Nature Communications* 6, 7751. doi:10.1038/ncomms8751.
- Karahanoglu, F.I., Van De Ville, D., 2017. Dynamics of large-scale fMRI networks: Deconstruct brain activity to build better models of brain function. *Current Opinion in Biomedical Engineering* 3, 28–36. doi:10.1016/j.cobme.2017.09.008.
- Khalidov, I., Fadili, J., Lazeyras, F., Van De Ville, D., Unser, M., 2011. Activelets: Wavelets for sparse representation of hemodynamic responses. *Signal processing* 91, 2810–2821.
- Kinany, N., Pirondini, E., Micera, S., Van De Ville, D., 2020. Dynamic Functional Connectivity of Resting-State Spinal Cord fMRI Reveals Fine-Grained Intrinsic Architecture. *Neuron* 108, 424–435.e4. doi:10.1016/j.neuron.2020.07.024.
- Lopes, R., Lina, J.M., Fahoum, F., Gotman, J., 2012. Detection of epileptic activity in fmri without recording the eeg. *Neuroimage* 60, 1867–1879.
- Meinshausen, N., Bühlmann, P., 2010. Stability selection. *Journal of the Royal Statistical Society: Series B (Statistical Methodology)* 72, 417–473.
- Petridou, N., Gaudes, C.C., Dryden, I.L., Francis, S.T., Gowland, P.A., 2013. Periods of rest in fMRI contain individual spontaneous events which are related to slowly fluctuating spontaneous activity. *Human Brain Mapping* 34, 1319–1329. doi:10.1002/hbm.21513.
- Raguet, H., Fadili, J., Peyré, G., 2013. A Generalized Forward-Backward Splitting. *SIAM Journal on Imaging Sciences* 6, 1199–1226. doi:10.1137/120872802.
- Schwarz, G., 1978. Estimating the Dimension of a Model. *Annals of Statistics* 6, 461–464. doi:10.1214/aos/1176344136.
- Tarun, A., Wainstein-Andriano, D., Sterpenich, V., Bayer, L., Perogamvros, L., Solms, M., Axmacher, N., Schwartz, S., Van De Ville, D., 2020. Nrem sleep stages specifically alter dynamical integration of large-scale brain networks. *Iscience* 24, 101923.
- Tibshirani, R., 1996. Regression Shrinkage and Selection Via the Lasso. *Journal of the Royal Statistical Society: Series B (Methodological)* 58, 267–288. doi:10.1111/j.2517-6161.1996.tb02080.x.
- Uruñuela, E., Jones, S., Crawford, A., Shin, W., Oh, S., Lowe, M., Caballero-Gaudes, C., 2020. Stability-Based Sparse Paradigm Free Mapping Algorithm for Deconvolution of Functional MRI Data. *Proceedings of the Annual International Conference of the IEEE Engineering in Medicine and Biology Society, EMBS 2020-July*, 1092–1095. doi:10.1109/EMBC44109.2020.9176137.
- Zöller, D., Sandini, C., Karahanoglu, F.I., Padula, M.C., Schaer, M., Eliez, S., Van De Ville, D., 2019. Large-scale brain network dynamics provide a measure of psychosis and anxiety in 22q11.2 deletion syndrome. *Biological Psychiatry: Cognitive Neuroscience and Neuroimaging* 4, 881–892.